Research Square

Preprints are preliminary reports that have not undergone peer review.
They should not be considered conclusive, used to inform clinical practice,
or referenced by the media as validated information.

Combined STN-DBS and acupuncture modulate cortico striatal oscillations and glymphatic function in anxious Parkinsonian rats

Xiaoyue Shen
Shandong University of Traditional Chinese Medicine
Weiqing Chen
Shandong First Medical University
Huajie Liu
Shandong Provincial Hospital
Liangshuo Li
Shandong First Medical University Third Affiliated Hospital & Affiliated Hospital of Shandong Academy of Medical Sciences
Shangfei Li
Shandong First Medical University
Ting Du
Shandong First Medical University
Yu Liu
Shandong First Medical University
Fei Su
Shandong First Medical University
Tao Xin
drxintao@yeah.net

Shandong Provincial QianFoShan Hospital

Article

Keywords:

Posted Date: June 14th, 2026

DOI: https://doi.org/10.21203/rs.3.rs-9934836/v1

License: This work is licensed under a Creative Commons Attribution 4.0 International License.
Read Full License

Additional Declarations: No competing interests reported.

Abstract

STN-DBS improves motor symptoms in Parkinson's disease (PD), but its effects on anxiety are variable. We tested whether manual acupuncture complements STN-DBS in A53T α-synuclein rats with anxiety-like behavior and examined paired scalp EEG in five DBS-treated patients with PD and anxiety. In rats, STN-DBS preferentially improved locomotion and modulated dorsomedial striatum-primary motor cortex coupling, whereas acupuncture preferentially reduced anxiety-like behavior and modulated dorsomedial striatum-medial prefrontal cortex coupling. Combined intervention improved both behavioral domains and shifted regional power, coherence and theta-gamma phase-amplitude coupling toward control profiles. Multi-omic and validation experiments implicated AQP4-associated glymphatic dysfunction: combined intervention improved cerebrospinal fluid influx, reduced striatal tracer retention, restored perivascular AQP4 polarization and reduced α-synuclein burden. TGN-020 partially attenuated behavioral benefit, supporting a contributory role for AQP4-associated clearance. Exploratory patient EEG showed additional prefrontal modulation during acupuncture with active STN-DBS. These findings support complementary circuit and clearance-related effects of combined intervention.

Introduction

Parkinson’s disease (PD) is a progressive neurodegenerative disorder in which non-motor symptoms are increasingly recognized as major determinants of disability and reduced quality of life [1]. Among these, anxiety is particularly important because it is common, clinically burdensome, frequently underrecognized, and may contribute to functional impairment to a degree comparable to that of motor symptoms in many patients [2,3]. Despite this clinical importance, anxiety in PD remains insufficiently understood and inadequately managed, indicating an unmet need beyond motor symptom control [4]. Subthalamic nucleus deep brain stimulation (STN-DBS) is an established treatment for advanced PD and remains highly effective for motor symptoms [5,6]. However, its effects on anxiety and related neuropsychiatric manifestations are less consistent, and emotional outcomes after surgery remain heterogeneous across patients [7]. This discrepancy suggests that modulation of canonical motor circuitry alone, while clinically effective for motor control, does not fully address the broader pathophysiology of PD with anxiety [8]. These limitations motivate the exploration of adjunctive interventions that act through pathways distinct from focal subcortical neuromodulation. Manual acupuncture represents one such candidate, in which somatic afferents at defined acupoints are mechanically stimulated. At the circuit level, recent studies have established that acupuncture stimulation engages defined classes of dorsal root ganglion sensory neurons that transmit signals to brainstem autonomic and modulatory nuclei [9,10]. From these brainstem relays, ascending projections reach higher cortical and limbic structures, with consistent engagement of the medial prefrontal cortex (mPFC), and limbic regions [11,12]. Notably, in PD, anxiety has been linked to altered prefrontal–striatal circuitry involved in threat appraisal, uncertainty processing, and top-down regulation of autonomic and affective responses, with the mPFC serving as a key cortical node for integrating emotional and executive control signals [13,14]. Although clinical evidence remains preliminary, a randomized controlled

trial has demonstrated that acupuncture significantly reduced Hamilton Anxiety Rating Scale scores in patients with PD compared with sham control and a systematic review further supported its anxiolytic potential among non-motor symptoms in PD [15,16]. These observations position acupuncture as a peripherally initiated intervention that engages prefrontal circuits through pathways anatomically distinct from focal STN-DBS, supporting their combination as a complementary strategy for PD with anxiety. Whether the two interventions engage dissociable circuit processes that together address motor and anxiety symptoms in PD remains to be established.

A circuit-level perspective is necessary to address this question. Abnormal activity within basal ganglia–thalamo–cortical motor loops is a core pathophysiological feature of PD and provides the principal framework for understanding the motor effects of STN-DBS, particularly in relation to pathological β synchronization and impaired motor output [17,18]. However, PD with anxiety is unlikely to be explained by motor-circuitry dysfunction alone. Converging clinical, neuroimaging and electrophysiological evidence indicates that anxiety in PD involves broader frontostriatal disturbances, with abnormalities in lower-frequency rhythms within prefrontal-and striatal- associated circuitry rather than a single symptomatic extension of motor pathology [19,20]. Beyond regional power, inter-regional synchronization and θ-γ phase–amplitude coupling have been implicated in both motor and affective dysfunction, providing a multi-level electrophysiological framework for dissecting circuit abnormalities in PD with anxiety [21,22]. This framework provides the basis for testing whether STN-DBS and acupuncture, given their distinct entry pathways, exert dissociable yet complementary effects on motor- and anxiety-associated circuit domains [23,24].

A circuit-based account, however, may remain incomplete without reference to the pathological substrate that sustains it. Excessive accumulation of α-synuclein (α-syn) is central to PD pathogenesis [25], and reflects an imbalance between production and clearance [26]. While intracellular degradation pathways have been studied extensively, extracellular clearance through the glymphatic system has emerged as a critical determinant of α-syn handling in the parkinsonian brain [27,28]. The glymphatic system is a glia-dependent perivascular transport pathway whose function depends on the polarized localization of aquaporin-4 (AQP4) at astrocytic endfeet [29,30]. Disturbance of this system has been linked to reduced clearance of pathological proteins and increased α-syn burden in Parkinsonian states [31]. Importantly, in PD with anxiety, pathological protein burden extends beyond the nigrostriatal system to striatal and other circuit-related regions implicated in affective dysfunction [32]. This raises the possibility that AQP4-dependent glympatic clarance represents a microenvironmental substract sustaining circuit-level abnormalities and might serve as a convergent point at which an effective combined intervention could act.

Building on these considerations, we hypothesized that combining STN-DBS with manual acupuncture would coordinately ameliorate motor and anxiety-related dysfunction in PD with anxiety by engaging dissociable yet complementary circuit- and clearance-related mechanisms. To test this hypothesis, we used A53T α-syn rats with restraint-induced anxiety to compare the behavioral and electrophysiological

effects of STN-DBS, acupuncture, and their combination. We further investigated the mechanistic basis through multi-omic profiling, glymphatic tracer experiments, AQP4 immunofluorescence and pharmacological AQP4 inhibition with TGN-020 and explored the translational relevance of prefrontal electrophysiological modulation in five DBS-treated patients with PD and anxiety using paired scalp EEG.

Results

Combined intervention ameliorates motor and anxiety-like deficits with dissociable contributions from each modality

We evaluated the behavioural and electrophysiological effects of STN-DBS, acupuncture and their combination using a predefined workflow that included viral delivery, electrode implantation, apomorphine rotation screening, intervention, local field potential recording, behavioural testing and terminal tissue collection (Fig. 1A). Recording electrodes targeted the mPFC, M1 and DMS, and the stimulating electrode was placed in the STN (Fig. 1B). Compared with NC animals, A53T rats showed reduced open-field total distance and centre exploration, fewer open-arm entries and reduced open-arm time in the elevated zero maze (Fig. 1C-E). STN-DBS increased total distance but did not significantly improve anxiety-related measures, whereas acupuncture increased centre exploration and open-arm time without significantly altering total distance. Combined intervention improved both behavioural domains, producing an effect profile not reproduced by either modality alone (n = 8 per group).

STN-DBS and acupuncture differentially modulate oscillatory power across cortico-striatal circuits

Power spectral analysis revealed distributed oscillatory abnormalities across the mPFC, M1 and DMS in A53T rats (Fig. 1F and G). In the mPFC, θ power was elevated in A53T rats and was reduced by acupuncture and combined intervention, whereas STN-DBS alone produced little change. In M1, β power was increased in A53T rats and reduced by all interventions, with a greater shift toward the NC profile after STN-DBS and combined intervention than after acupuncture alone. In the DMS, θ and β power were elevated. DMS θ power was reduced by STN-DBS and most strongly by combined intervention, whereas acupuncture alone had little effect; DMS β power was reduced across all intervention groups, with the combined group closest to the NC profile. Thus, STN-DBS preferentially modulated motor-related β abnormalities in M1 and DMS, whereas acupuncture more prominently affected prefrontal θ activity. Combined intervention engaged both domains.

Combined intervention rebalances pathway- and frequency-specific coherence abnormalities

A53T rats showed abnormal inter-regional coherence across the cortico-striatal network (Fig. 2A-E). In the DMS-M1 pathway, β-band coherence was increased relative to NC animals and was attenuated after intervention, with STN-DBS producing a greater reduction than acupuncture and combined intervention

shifting the profile closest to NC (Fig. 2A, D and E). A similar β-dominant abnormality was observed in the M1-mPFC pathway and was most strongly reduced in the combined group (Fig. 2B, D and E). In the DMS-mPFC pathway, θ-band coherence was increased in A53T rats and attenuated by both STN-DBS and acupuncture, with the largest reduction after combined intervention (Fig. 2C-E). These data indicate pathway- and frequency-specific coherence abnormalities, with STN-DBS preferentially affecting DMS-M1 β coherence and acupuncture contributing more prominently to DMS-mPFC θ coherence.

STN-DBS and acupuncture differentially reduce local prefrontal and inter-regional phase-amplitude coupling

Phase-amplitude coupling (PAC) was analysed before and after intervention in the STN-DBS, acupuncture and combined-intervention groups (Fig. 3A-F). In the mPFC, local θ-phase to γ-amplitude coupling showed no significant change after STN-DBS alone but was reduced by acupuncture and most strongly by combined intervention (Fig. 3A-C). By contrast, DMS-M1 θ–γ coupling showed no significant change after acupuncture alone but was reduced by STN-DBS and most strongly by combined intervention (Fig. 3D-F). Thus, acupuncture preferentially attenuated local mPFC θ–γ coupling, whereas STN-DBS preferentially attenuated inter-regional DMS-M1 θ–γ coupling. Combined intervention produced the largest reductions in both measures.

Striatal multi-omic profiling implicates AQP4-associated clearance dysfunction in the PD-anxiety model

Untargeted metabolomic and transcriptomic profiling of striatal tissue from NC and A53T rats identified disease-associated molecular alterations. Metabolomic analysis showed group separation, with differential metabolites mapping to energy metabolism, lipid metabolism, oxidative stress, amino acid metabolism and proteostasis-related pathways (Fig. 4A-E). Transcriptomic profiling showed a parallel disease-associated shift, with Aqp4 among the differentially expressed genes (Fig. 4F-H). Weighted gene co-expression network analysis identified A53T-associated modules and disease-linked hub genes (Fig. 4I-K). Stratification by Aqp4 expression revealed distinct transcriptional profiles, including changes in glymphatic-associated genes such as Dmd and Dtna (Fig. 4L-N). Enrichment of AQP4-associated genes implicated signalling and neurodevelopmental processes, including G protein-coupled receptor signalling, cAMP-mediated signalling, cognition, learning and memory, and telencephalon development (Fig. 4O and P). Analysis of a public single-cell RNA-sequencing dataset provided exploratory human support for an AQP4-associated PD context (Fig. 4Q-S). These analyses nominated AQP4-associated regulation for subsequent functional assessment of CSF influx, striatal clearance, perivascular AQP4 polarization and α-syn pathology.

Combined intervention improves glymphatic transport and perivascular AQP4 polarization

Because multi-omic profiling implicated AQP4-associated clearance dysfunction, we examined brain fluid transport. CSF tracer assays showed reduced parenchymal entry of TRITC-labelled 4 kDa dextran and FITC-labelled 40 kDa dextran in A53T rats, indicating impaired CSF influx (Fig. 5A, B and D-G). This deficit was attenuated after intervention, with combined STN-DBS and acupuncture producing the closest shift toward NC. Striatal clearance was also impaired: after intrastriatal injection of FITC-labelled 2000 kDa dextran, A53T rats showed increased tracer retention, which was reduced most strongly in the combined group (Fig. 5C, H and I). Immunofluorescence showed increased GFAP immunoreactivity and disrupted perivascular AQP4 localization in the DMS and substantia nigra of A53T rats; combined intervention produced the most evident restoration of perivascular AQP4 polarization (Fig. 5J and K).

Combined intervention attenuates α-syn pathology and supports nigrostriatal preservation

We next examined whether AQP4-associated transport abnormalities were accompanied by α-syn accumulation and nigrostriatal pathology. In A53T rats, TH immunoreactivity was reduced in the substantia nigra and striatum, whereas α-syn labelling was increased in the substantia nigra (Fig. 6A-D). These abnormalities were attenuated after intervention, with combined intervention showing the greatest preservation of TH signal and the strongest reduction in α-syn burden. CD31/α-syn double labelling further showed reduced vascular CD31 signal and increased α-syn accumulation in the substantia nigra of A53T rats, both most clearly improved after combined intervention (Fig. 6E and F). Consistently, striatal immunoblotting showed reduced AQP4 and TH expression in A53T rats compared with NC rats. Both STN-DBS and acupuncture partially restored these proteins, and combined intervention produced the most consistent increase toward the NC profile (Fig. 6G). Together, these findings indicate reduced α-syn burden and partial preservation of dopaminergic and vascular integrity, with WB evidence supporting recovery of AQP4 and TH expression.

Pharmacological AQP4 inhibition attenuates the behavioural benefit of combined intervention

To test whether AQP4-associated mechanisms contributed to the behavioural effect of combined STN-DBS and acupuncture, A53T rats receiving combined intervention were treated with the AQP4 inhibitor TGN-020 or vehicle. In the open-field test, TGN-020 reduced both total distance and centre distance relative to vehicle-treated animals (Fig. 7A and B), indicating partial attenuation of the combined-intervention benefit. Across groups, AQP4 expression was positively correlated with total distance, centre distance, open-arm entries and open-arm time ratio, and negatively correlated with DMS θ and β power and β-band DMS-M1 and M1-mPFC coherence (Fig. 7C and D). These findings support AQP4-associated glymphatic function as a contributing, but not exclusive, mechanism linking behavioural improvement with reduced cortico-striatal electrophysiological abnormalities.

Acupuncture further modifies prefrontal electrophysiology during active STN-DBS

We performed a paired exploratory EEG analysis in DBS-treated patients with PD and anxiety to examine whether the prefrontal electrophysiological effects observed in rats were detectable clinically. Six patients were enrolled; one was excluded because of excessive bad EEG channels, leaving five for analysis. Resting-state EEG was recorded under DBS_OFF, DBS_ON and DBS_ON_ACU conditions (Fig. 8A and B). Frontal/prefrontal θ power was reduced under DBS_ON_ACU compared with DBS_OFF, whereas DBS_ON alone did not significantly differ from DBS_OFF. Low-β power was reduced under both DBS_ON and DBS_ON_ACU, whereas high-β power did not differ across conditions (Fig. 8C). Prefrontal θ–γ PAC was condition-dependent: DBS_ON reduced θ–γ coupling relative to DBS_OFF, and DBS_ON_ACU produced an additional reduction, most clearly at Fp1 (Fig. 8D). Coherence analysis showed that DBS_ON reduced frontal/prefrontal-to-central coherence relative to DBS_OFF, with additional reductions during DBS_ON_ACU across selected electrode pairs (Fig. 8E). These exploratory clinical EEG data suggest that acupuncture during active STN-DBS further modulates prefrontal electrophysiological activity, consistent with the preclinical circuit dissociation.

Discussion

The present study examined whether manual acupuncture could complement STN-DBS in PD with anxiety-like features. In A53T α-synuclein rats exposed to repeated restraint stress, combined intervention improved both locomotor impairment and anxiety-like behavior, whereas each single intervention showed a more restricted behavioral profile. Electrophysiological analyses suggested partially dissociable circuit effects: STN-DBS preferentially modulated DMS–M1 motor-related coupling, whereas acupuncture more prominently affected prefrontal activity and DMS–mPFC coupling. Multi-omic profiling, glymphatic tracer experiments and pathological analyses implicated AQP4-associated clearance dysfunction as a biological process linked to the combined response. TGN-020 partially attenuated the behavioral benefit, supporting AQP4-associated glymphatic function as a contributor rather than the sole mediator. Exploratory EEG in DBS-treated patients further suggested that acupuncture during active STN-DBS can modulate prefrontal electrophysiological activity.

The dissociable behavioral effects of STN-DBS and acupuncture suggest that motor and anxiety-related manifestations in this model are associated with partially separable circuit abnormalities. In A53T rats with anxiety-like behavior, electrophysiological disturbances were detected across mPFC, DMS and M1 recordings, involving regional oscillatory power, inter-regional coherence, and phase–amplitude coupling. These findings support the view that PD with anxiety is not adequately explained by motor-circuit dysfunction alone but involves broader cortico-striatal network alterations that include motor-associated and prefrontal-associated components [33–35]. Within this framework, STN-DBS preferentially improved locomotor deficits and more strongly modulated DMS–M1 motor-related electrophysiological coupling, whereas acupuncture preferentially attenuated anxiety-like behavior and more clearly modulated local mPFC rhythmic coupling and DMS–mPFC electrophysiological coupling. This pattern is consistent with

the established effect of STN-DBS on pathological motor-network synchronization [36–38] and with evidence implicating prefrontal–striatal dysfunction in anxiety and other neuropsychiatric manifestations of PD [39,40].

The circuit specificity of these effects was further supported by pathway- and frequency-dependent changes in coherence and phase–amplitude coupling. β-dominant abnormalities were mainly observed in the DMS–M1 and M1–mPFC recording pairs, consistent with the contribution of β synchronization to parkinsonian motor dysfunction [41,42]. By contrast, the DMS–mPFC pathway showed a θ-band coherence abnormality, indicating a distinct prefrontal–striatal electrophysiological domain. STN-DBS more clearly reduced DMS–M1 β coherence and DMS-driven θ–γ coupling with M1, whereas acupuncture reduced local mPFC θ–γ coupling. In the DMS–mPFC pathway, both STN-DBS and acupuncture attenuated θ coherence, while combined intervention produced the largest reduction. Because coherence and phase–amplitude coupling do not establish anatomical connectivity or directionality, these findings should be interpreted as evidence of functional electrophysiological coupling rather than direct evidence of defined anatomical pathways. Nevertheless, the coordinated benefit of combined intervention can be understood as broader modulation of disease-relevant circuit dysfunction, with STN-DBS primarily acting on motor-associated cortico-striatal abnormalities and acupuncture preferentially engaging prefrontal electrophysiological abnormalities related to anxiety-like behavior.

Beyond circuit-level modulation, the data implicate AQP4-associated glymphatic function as a clearance-related process linked to the response to combined intervention. PD pathogenesis involves α-synuclein accumulation, which may reflect both abnormal aggregation and impaired clearance [43–46]. In the present model, pathology extended beyond the substantia nigra to the striatum, where electrophysiological abnormalities were also detected. Multi-omic profiling identified disease-associated changes involving astroglial responses, vascular–glial homeostasis and Aqp4-related regulation. This signal is biologically relevant because polarized AQP4 at astrocytic endfeet supports perivascular fluid exchange and interstitial solute movement [47–49]. Consistently, A53T rats showed reduced CSF tracer influx, increased striatal tracer retention, increased GFAP immunoreactivity and disrupted perivascular AQP4 polarization.

Combined STN-DBS and acupuncture attenuated these abnormalities and was associated with reduced α-synuclein burden, preserved TH expression and partial recovery of CD31-associated vascular signal. These observations are consistent with previous studies linking glymphatic impairment to PD and synucleinopathy [50–53]. They also suggest that the combined intervention was associated with improvement in the vascular–glial and clearance-related microenvironment, in addition to electrophysiological modulation. However, the evidence should be interpreted cautiously. TGN-020 partially weakened the behavioral benefit, and AQP4 expression correlated with behavioral and electrophysiological readouts, but these data do not establish a complete causal sequence from glymphatic restoration to circuit normalization [54].

The circuit and clearance findings are therefore best viewed as interacting components of the treatment response. STN-DBS and acupuncture appear to engage partially dissociable electrophysiological

domains, while the combined intervention also improves an AQP4-associated microenvironment that may influence extracellular solute movement and α-synuclein handling. Improved clearance-related transport may reduce protein retention, preserve vascular–glial integrity and create a more permissive biological context for cortico-striatal network recovery. This integrated interpretation may explain why combined intervention produced broader effects than either modality alone.

The clinical EEG experiment provides preliminary translational support for the prefrontal component of this model. Although scalp EEG cannot resolve striatal or subthalamic activity, acupuncture during active STN-DBS was associated with additional changes in frontal/prefrontal θ power, low-β power, θ–γ phase–amplitude coupling and frontal/prefrontal–central coherence. These findings are directionally consistent with the preclinical observation that acupuncture affects prefrontal electrophysiological coupling. The small sample size, self-controlled design and single-session intervention preclude conclusions regarding sustained clinical benefit or therapeutic efficacy. The clinical data should therefore be viewed as exploratory evidence that prefrontal electrophysiological processes remain modifiable during active STN-DBS.

Several limitations should be acknowledged. The A53T plus repeated restraint stress model captures selected features of PD with anxiety but does not reproduce the full biological and clinical complexity of the human disorder. The electrophysiological analysis was restricted to the mPFC–DMS–M1 network and did not assess wider limbic, thalamic or brainstem systems. The TGN-020 and correlation analyses support involvement of AQP4-associated processes but do not establish a complete causal sequence linking clearance failure, α-synuclein retention and circuit abnormality. The multi-omic data were hypothesis-generating. The clinical component was exploratory, and its small sample size and single-session design do not permit inference regarding sustained symptom improvement.

In summary, the present data support a model in which PD with anxiety-like features involves interactions among motor-network pathology, prefrontal-network dysregulation and clearance-related microenvironmental disturbance. STN-DBS was aligned more closely with the DMS–M1 motor-related cortico-striatal domain, whereas acupuncture was aligned more closely with prefrontal rhythmic activity and DMS–mPFC coupling. Their combination was associated with broader benefit by engaging both domains and improving AQP4-associated transport, perivascular polarization, and pathological protein handling. The clinical EEG findings do not establish therapeutic efficacy, but they support the preliminary translational relevance of testing combined STN-DBS and acupuncture in controlled studies of persistent non-motor symptoms in DBS-treated patients with PD.

Materials and methods

Animals and model generation

Adult male Sprague-Dawley rats weighing 220–250 g were obtained from Jinan Pengyue Experimental Animal Breeding Co., Ltd. Rats were housed under specific pathogen-free conditions with a 12-h light/dark cycle, temperature of 22 ± 2°C, 50–60% humidity and ad libitum access to food and water. All

procedures were approved by the Animal Experiment Ethics Committee of the First Affiliated Hospital of Shandong First Medical University (LCYJLL2022(009)) and were performed in accordance with the National Institutes of Health Guide for the Care and Use of Laboratory Animals.

PD with anxiety-like features was induced by bilateral substantia nigra injection of rAAV1/2-hSyn-A30P-A53T-αSyn followed by repeated restraint stress. Rats received stereotaxic injection of rAAV1/2-hSyn-A30P-A53T-αSyn (5.03×10^{12} genome particles/ml; Braincase, Shenzhen, China) or empty control vector (7.02×10^{12} genome particles/ml; Braincase). Under isoflurane anaesthesia, viral suspension was injected bilaterally into the substantia nigra (AP -5.2 mm, ML ± 2.0 mm, DV -7.5 mm) at 0.1 μl/min, with 2 μl delivered per side. The needle was left in place for 10 min before withdrawal. Beginning the day after viral injection, rats underwent restraint stress for 15 min daily for 14 days.

Experimental design and interventions

Rats were randomly assigned to NC, A53T, A53T_DBS, A53T_ACU and A53T_CO groups. NC rats received empty-vector injection, whereas all A53T groups received A53T-α-synuclein injection. A53T_DBS rats received active STN-DBS and sham acupuncture, in which sterile needles were inserted into muscle sites adjacent to the selected acupoints but outside the defined acupoint regions. A53T_ACU rats received manual acupuncture and were implanted with an STN electrode that remained switched off. A53T_CO rats received both active STN-DBS and manual acupuncture. Sample sizes are provided in the figure legends.

For electrophysiological experiments, a chronic bipolar stimulation electrode was implanted into the right STN (AP -3.6 mm, ML + 2.5 mm, DV -7.8 mm), a 4 × 4 microwire array into the DMS (AP + 0.2 mm, ML -2.0 mm, DV -4.5 mm), and screw electrodes over the mPFC (AP + 2.7 mm, ML -0.8 mm, DV -2.5 mm) and M1 (AP + 1.0 mm, ML -2.5 mm, DV -2.0 mm). Ground and reference electrodes were placed over the cerebellar region. STN-DBS was delivered for 7 days beginning in week 5 after model induction using 130 Hz stimulation, 60 μs pulse width and 50–100 μA current intensity. Manual acupuncture was administered once daily for 7 days at bilateral LR3, KI3 and ST36, localized according to experimental acupuncture standards and previous studies [55,56]. Sterile needles (0.25 × 25 mm; Fujian Zhongjing Pharmaceutical Co., Ltd.) were inserted to 2–3 mm at LR3/KI3 and 4 mm at ST36 and rotated 90° alternately in both directions for 15 s at 5-min intervals. Sham acupuncture followed the same handling schedule at adjacent non-acupoint muscle sites.

The experimental timeline comprised viral injection at week 0, recovery and A53T-α-synuclein expression during weeks 1–3, electrode implantation at week 3, restraint stress during weeks 3–4, intervention at week 5 and analyses from week 6. The TGN-020 experiment used an independent cohort processed through the same timeline [57].

Behavioural testing

Behavioural testing was performed after intervention by experimenters blinded to group allocation. In the open-field test, rats explored a black arena (100 × 100 × 40 cm) for 5 min. Total distance was used as a locomotor index and centre-zone exploration as an anxiety-related index. In the elevated zero maze, rats explored the maze for 5 min, and open-arm entries and percentage of time spent in open arms were quantified using an automated video-tracking system.

Local field potential recording and analysis

Local field potentials were recorded simultaneously from the mPFC, DMS and M1 in awake, freely moving rats using an OmniPlex system (Plexon, Dallas, TX, USA). Recordings were obtained before and within 1 week after intervention. Signals were acquired at 40 kHz, band-pass filtered at 0.5–100 Hz, notch filtered at 50 Hz and downsampled to 1000 Hz. Video was synchronized with electrophysiological recordings, and 15 min of artefact-free quiet-wakefulness data per animal were analysed. Power spectral density was calculated in MATLAB using Welch's method with 2-s windows, 50% overlap and 0.5-Hz resolution. Relative power was normalized to total power from 1-100 Hz and analysed in θ, β and γ bands. Magnitude-squared coherence was calculated for predefined DMS-M1, M1-mPFC and DMS-mPFC pairs. PAC was quantified using a Hilbert transform-based modulation index.

RNA sequencing, metabolomics and public single-cell analysis

Striatal tissue was collected after behavioural and electrophysiological testing, snap-frozen and stored at -80°C. RNA sequencing and untargeted metabolomics were performed in NC and A53T rats to identify disease-associated molecular alterations. The bioinformatic analyses included sequencing data generated in this study, comprising four PD-model samples and six control samples, together with the public single-cell dataset GSE184950.

For RNA sequencing, total RNA was extracted, quality-controlled and sequenced using a high-throughput platform. Raw transcriptomic data were processed to obtain normalized mRNA expression matrices. Differential expression, hierarchical clustering and pathway enrichment were performed between NC and A53T groups; GEO expression matrices were processed using limma. WGCNA was performed using the top 25% most variable genes to identify disease-associated modules. Modules were merged using a dynamic tree cut threshold of 0.25, and module eigengenes, module membership and gene significance were used to identify hub genes and AQP4-related transcriptional networks. For AQP4-stratified analyses, samples were divided into AQP4-high and AQP4-low subgroups for differential expression and enrichment analyses.

For metabolomics, differential metabolites were identified between NC and A53T groups, followed by clustering and pathway enrichment. Metabolite annotation and pathway-related database mapping were performed using MetaboAnalyst (https://www.metaboanalyst.ca/). Single-cell data from GSE184950 were obtained from GEO and analysed in R using Seurat version 4.3.0.1. Cells expressing fewer than 200 or more than 5000 genes were excluded. Data were normalized, scaled and analysed by PCA. Harmony

was used to integrate 18 datasets and correct batch effects. UMAP visualization and graph-based clustering were performed using Harmony-corrected dimensions, with clustering resolution set to 0.7. Cell types were annotated using canonical marker genes, literature evidence and CellMarker 2.0.

Single-cell differential expression was performed using FindMarkers with logfc.threshold = 0.25 and min.pct = 0.1. Wilcoxon rank-sum tests and Benjamini-Hochberg correction were used. Differentially expressed genes were defined as $P < 0.01$ and $|\log2FC| > 1$. Gene Ontology and gene set enrichment analyses were performed using clusterProfiler. These public single-cell analyses were used as exploratory external support and not as direct evidence of striatal glymphatic dysfunction.

Glymphatic tracer experiments

Glymphatic tracer experiments assessed CSF influx and striatal solute clearance. For CSF influx assays, FITC-labelled 40 kDa dextran and TRITC-labelled 4 kDa dextran were dissolved in artificial CSF as a 0.5% mixture. A 30-gauge needle was advanced into the cisterna magna, and 10 μl tracer solution was infused at 0.1 μl/min. Rats were perfused 30 min later, and 100-μm coronal brain sections were imaged by fluorescence microscopy. For striatal clearance assays, FITC-labelled 2000 kDa dextran was injected into the DMS (AP + 0.5 mm, ML + 2.0 mm, DV -3.0 mm; 2 μl per side, 0.2–0.3 μl/min). Rats were perfused 2 h later. Fluorescence intensity was quantified in predefined regions of interest using ImageJ by a blinded experimenter.

Immunofluorescence, immunohistochemistry, and western blotting

After transcardial perfusion with PBS, brains were paraffin-embedded and cut into 4-μm coronal sections. Sections were processed for antibodies against AQP4 (Abclonal, A11210; 1:500), GFAP (Abclonal, A28062; 1:500), TH (Abclonal, A25683; 1:500), α-synuclein (Proteintech, 10842-1-AP; 1:300) and CD31/PECAM1 (Abclonal, A19014; 1:500). AQP4/GFAP double labelling was performed in the DMS and substantia nigra, and TH/α-synuclein and CD31/α-synuclein double labelling in the substantia nigra. TH immunohistochemistry was performed in the substantia nigra and striatum using DAB visualization. Images were acquired under identical exposure settings and quantified in ImageJ by a blinded experimenter.

For western blotting, striatal tissue was homogenized in RIPA buffer, centrifuged and quantified using a BCA assay. Equal amounts of protein were separated by SDS-PAGE, transferred to PVDF membranes, and incubated with antibodies against AQP4 (1:1000), TH (1:1000) and β-actin (1:5000). Bands were visualized using ECL, quantified in ImageJ and normalized to β-actin.

TGN-020 intervention and correlation analyses

To test whether AQP4-associated mechanisms contributed to the effect of combined intervention, an independent cohort of A53T_CO rats received intraperitoneal TGN-020 (100 mg/kg; HY-W008574, MedChemExpress, USA) or vehicle. Model induction, intervention and behavioural testing were otherwise

identical. Open-field testing assessed total distance and centre exploration. Animal-level behavioural, electrophysiological, tracer-derived, histological and biochemical measurements were matched for correlation analyses. Associations between AQP4-related measures and behavioural or electrophysiological readouts were assessed using Pearson or Spearman correlation according to data distribution.

Clinical participants, EEG recording and analysis

A single-centre, prospective, self-controlled observational study was conducted in clinically stable patients with PD and comorbid anxiety after bilateral STN-DBS. Patients were recruited between October 2024 and October 2025. The study was approved by the local ethics committee (LCYJLL2022(009)), and all participants provided written informed consent. This component was designed as an exploratory translational electrophysiological analysis rather than an efficacy trial.

PD was diagnosed according to the Chinese diagnostic criteria for PD (2016 edition), and anxiety was defined by DSM-5 criteria or Hamilton Anxiety Rating Scale score ≥ 14. Eligible participants were 50–80 years old, right-handed, at least 6 months post-STN-DBS and on stable medication. Six patients were enrolled; one was excluded because of excessive bad EEG channels, leaving five patients for paired analysis. Resting-state EEG was recorded under DBS_OFF, DBS_ON and DBS_ON_ACU conditions. DBS_ON used each patient's clinical stimulation parameters; DBS_ON_ACU combined active STN-DBS with single-session manual acupuncture, without medication or stimulation changes. Bilateral LR3, KI3 and ST36 were stimulated using sterile needles, manually manipulated to elicit deqi [58], retained for 30 min and manipulated every 10 min. No electrical stimulation was applied.

EEG was acquired for 20 min per condition after a 5-min adaptation period using a 32-channel 10–20 montage, referenced to A1/A2 with Fpz as ground. Signals were sampled at 1000 Hz with 0.1–100 Hz bandwidth and 50-Hz notch filtering. Preprocessing was performed in Python using MNE-Python, NumPy and SciPy. Signals were re-referenced to the bilateral earlobe average, filtered and segmented into 2-s epochs. DBS-related artefacts were removed during preprocessing 38. Ocular, muscle, and cardiac artefacts were removed using independent component analysis with ICLabel-assisted classification, and bad channels were repaired by spherical spline interpolation. Power spectral density, θ–γ PAC and coherence were calculated from preprocessed EEG. Spectral analyses focused on θ, low-β and high-β bands. θ–γ coupling was quantified at Fp1 and Fp2, and frontal/prefrontal-to-central coherence was assessed between Fp1/Fp2/F3/F4/Fz and C3/C4/Cz.

Statistical analysis

Data are presented as mean ± SEM unless otherwise stated. Statistical analyses were performed using GraphPad Prism. Data distribution was assessed before test selection. For multiple independent groups, one-way ANOVA with Tukey's post hoc test or Kruskal-Wallis test with Dunn's correction was used. Two-group comparisons were performed using unpaired two-tailed Student's t-test or Mann-Whitney U test. Clinical EEG data were analysed using repeated-measures ANOVA or Friedman test with paired post hoc comparisons. A two-sided $P < 0.05$ was considered significant.

Declarations

Competing interests

The authors declare no competing financial or non-financial interests.

Funding

This work was supported by Key Research and Development Program in Shandong Province (ZR2025ZD13), Taishan Scholar Program of Shandong Province under Grant (202312360 and 20230659).

Author Contribution

X.S. and W.C. conducted most of the experiments and drafted the manuscript. H.L. and S.L. contributed to conducted clinical assessments. L.L. and T.D. contributed to sample collection and data visualization. X.T and F.S. conceived and designed the study. All authors reviewed and approved the final version of the manuscript.

Acknowledgement

This work was supported by Key Research and Development Program in Shandong Province (ZR2025ZD13), Taishan Scholar Program of Shandong Province under Grant (202312360 and 20230659), We would like to thank the Joint Innovation Team for Clinical & Basic Research of Shandong First Medical University (Shandong Academy of Medical Sciences) (No. 202404); Shandong Provincial Key Laboratory of Brain Science (No. PKL2024C12).

References

1. Chaudhuri, K.R., Healy, D.G. & Schapira, A.H. Non-motor symptoms of Parkinson's disease: diagnosis and management. Lancet Neurol 5, 235–245 (2006).
2. Weintraub, D., et al. The neuropsychiatry of Parkinson's disease: advances and challenges. Lancet Neurol 21, 89–102 (2022).
3. Blundell, E.K., Grover, L.E., Stott, J. & Schrag, A. The experience of Anxiety for people with Parkinson's disease. NPJ Parkinsons Dis 9, 75 (2023).
4. Pontone, G.M., et al. Report from a multidisciplinary meeting on anxiety as a non-motor manifestation of Parkinson's disease. NPJ Parkinsons Dis 5, 30 (2019).
5. Asriyants, S.V., Tomskiy, A.A., Gamaleya, A.A. & Pronin, I.N. Deep brain stimulation of the subthalamic nucleus for parkinson's disease: awake vs asleep. Zh Vopr Neirokhir Im N N Burdenko

85, 117–121 (2021).
6. Deuschl, G. & Agid, Y. Subthalamic neurostimulation for Parkinson's disease with early fluctuations: balancing the risks and benefits. Lancet Neurol 12, 1025–1034 (2013).
7. Muldmaa, M., et al. Deciphering the effects of STN DBS on neuropsychiatric fluctuations in Parkinson's disease. NPJ Parkinsons Dis 10, 205 (2024).
8. Kurtis, M.M., Rajah, T., Delgado, L.F. & Dafsari, H.S. The effect of deep brain stimulation on the non-motor symptoms of Parkinson's disease: a critical review of the current evidence. NPJ Parkinsons Dis 3, 16024 (2017).
9. Li, Q., et al. Effect of acupuncture for non-motor symptoms in patients with Parkinson's disease: A systematic review and meta-analysis. Front Aging Neurosci 14, 995850 (2022).
10. Li, K., et al. Electroacupuncture for motor dysfunction and constipation in patients with Parkinson's disease: a randomised controlled multi-centre trial. EClinicalMedicine 56, 101814 (2023).
11. Lin, J., Kong, Y., Chen, H., Ding, X. & Zhou, W. Effects of acupuncture on sleep quality in patients with Parkinson's disease: A systematic review and meta-analysis. Clin Rehabil 38, 478–496 (2024).
12. Kühn, A.A., et al. Pathological synchronisation in the subthalamic nucleus of patients with Parkinson's disease relates to both bradykinesia and rigidity. Exp Neurol 215, 380–387 (2009).
13. Liu, S., et al. Somatotopic Organization and Intensity Dependence in Driving Distinct NPY-Expressing Sympathetic Pathways by Electroacupuncture. Neuron 108, 436–450.e437 (2020).
14. Liu, S., et al. A neuroanatomical basis for electroacupuncture to drive the vagal-adrenal axis. Nature 598, 641–645 (2021).
15. Huang, W., et al. Characterizing acupuncture stimuli using brain imaging with FMRI–a systematic review and meta-analysis of the literature. PLoS One 7, e32960 (2012).
16. Yeo, S., et al. Acupuncture on GB34 activates the precentral gyrus and prefrontal cortex in Parkinson's disease. BMC Complement Altern Med 14, 336 (2014).
17. Carey, G., et al. Neuroimaging of Anxiety in Parkinson's Disease: A Systematic Review. Mov Disord 36, 327–339 (2021).
18. Oosterwijk, C.S., Vriend, C., Berendse, H.W., van der Werf, Y.D. & van den Heuvel, O.A. Anxiety in Parkinson's disease is associated with reduced structural covariance of the striatum. J Affect Disord 240, 113–120 (2018).
19. Fan, J.Q., et al. Effectiveness of Acupuncture for Anxiety Among Patients With Parkinson Disease: A Randomized Clinical Trial. JAMA Netw Open 5, e2232133 (2022).
20. Zhang, A., et al. Acupuncture for the Treatment of Neuropsychiatric Symptoms in Parkinson's Disease: A Systematic Review and Meta-Analysis. Complement Ther Med 80, 103020 (2024).
21. Wang, X., et al. Altered putamen functional connectivity is associated with anxiety disorder in Parkinson's disease. Oncotarget 8, 81377–81386 (2017).
22. Carey, G., et al. Anxiety in Parkinson's disease is associated with changes in the brain fear circuit. Parkinsonism Relat Disord 80, 89–97 (2020).

23. Stein, E. & Bar-Gad, I. β oscillations in the cortico-basal ganglia loop during parkinsonism. Exp Neurol 245, 52–59 (2013).
24. Betrouni, N., et al. Anxiety in Parkinson's disease: A resting-state high density EEG study. Neurophysiol Clin 52, 202–211 (2022).
25. Calabresi, P., et al. Alpha-synuclein in Parkinson's disease and other synucleinopathies: from overt neurodegeneration back to early synaptic dysfunction. Cell Death Dis 14, 176 (2023).
26. Bramson, B., den Ouden, H.E., Toni, I. & Roelofs, K. Improving emotional-action control by targeting long-range phase-amplitude neuronal coupling. Elife 9 (2020).
27. Luo, Q., et al. Theta band activity in response to emotional expressions and its relationship with gamma band activity as revealed by MEG and advanced beamformer source imaging. Front Hum Neurosci 7, 940 (2013).
28. Nedergaard, M. & Goldman, S.A. Glymphatic failure as a final common pathway to dementia. Science 370, 50–56 (2020).
29. Tamtaji, O.R., Behnam, M., Pourattar, M.A., Jafarpour, H. & Asemi, Z. Aquaporin 4: A key player in Parkinson's disease. J Cell Physiol 234, 21471–21478 (2019).
30. Lapshina, K.V. & Ekimova, I.V. Aquaporin-4 and Parkinson's Disease. Int J Mol Sci 25 (2024).
31. Xun, Z., Sowell, R.A., Kaufman, T.C. & Clemmer, D.E. Quantitative proteomics of a presymptomatic A53T alpha-synuclein Drosophila model of Parkinson disease. Mol Cell Proteomics 7, 1191–1203 (2008).
32. Alqahtani, T., et al. Mitochondrial dysfunction and oxidative stress in Alzheimer's disease, and Parkinson's disease, Huntington's disease and Amyotrophic Lateral Sclerosis -An updated review. Mitochondrion 71, 83–92 (2023).
33. Derosiere, G., et al. Fronto-motor circuits linked to effort-based decision-making and apathy in healthy subjects. Commun Biol 8, 1320 (2025).
34. De Micco, R., et al. Connectivity Correlates of Anxiety Symptoms in Drug-Naive Parkinson's Disease Patients. Mov Disord 36, 96–105 (2021).
35. de Hemptinne, C., et al. Prefrontal Physiomarkers of Anxiety and Depression in Parkinson's Disease. Front Neurosci 15, 748165 (2021).
36. Alhourani, A., et al. Network effects of deep brain stimulation. J Neurophysiol 114, 2105–2117 (2015).
37. de Hemptinne, C., et al. Therapeutic deep brain stimulation reduces cortical phase-amplitude coupling in Parkinson's disease. Nat Neurosci 18, 779–786 (2015).
38. Whitmer, D., et al. High frequency deep brain stimulation attenuates subthalamic and cortical rhythms in Parkinson's disease. Front Hum Neurosci 6, 155 (2012).
39. Swinnen, B., et al. Basal ganglia theta power indexes trait anxiety in people with Parkinson's disease. Brain 148, 1228–1241 (2025).

40. Hodnik, T., Roytman, S., Bohnen, N.I. & Marusic, U. Beta-Gamma Phase-Amplitude Coupling as a Non-Invasive Biomarker for Parkinson's Disease: Insights from Electroencephalography Studies. Life (Basel) 14 (2024).
41. Wang, W. Brain network features based on theta-gamma cross-frequency coupling connections in EEG for emotion recognition. Neurosci Lett 761, 136106 (2021).
42. Li, Y., Li, S., Tang, Y., Hao, S. & Zhang, D. Causal evidence for the role of prefrontal theta oscillations in emotion regulation using neurofeedback training. Neuroimage 320, 121457 (2025).
43. Du, X.Y., Xie, X.X. & Liu, R.T. The Role of α-Synuclein Oligomers in Parkinson's Disease. Int J Mol Sci 21 (2020).
44. Carey, G., et al. Anxiety in Parkinson's Disease Is Associated with Changes in Brain Structural Connectivity. J Parkinsons Dis 13, 989–998 (2023).
45. Lv, Y., et al. Glymphatic dysfunction in Parkinson's disease: Aging-associated impairments, imaging biomarkers, and therapeutic strategies. Ageing Res Rev 114, 102995 (2026).
46. Ho, M.S. Clearance Pathways for α-Synuclein in Parkinson's Disease. J Neurochem 169, e70124 (2025).
47. Lian, T., et al. Parkinson's disease with anxiety: clinical characteristics and their correlation with oxidative stress, inflammation, and pathological proteins. BMC Geriatr 24, 433 (2024).
48. Perepezko, K., et al. Anxiety in Parkinson's Disease: A Systematic Review of Neuroimaging Studies. J Neuropsychiatry Clin Neurosci 33, 280–294 (2021).
49. Braun, M., et al. Aquaporin-4 mis-localization slows glymphatic clearance of α-synuclein and promotes α-synuclein pathology and aggregate propagation. bioRxiv (2024).
50. Lopes, D.M., et al. The influence of the glymphatic system on α-synuclein propagation: the role of aquaporin-4. Brain 148, 4519–4531 (2025).
51. Qin, J., et al. The effects of aquaporin-4 polymorphisms on glymphatic function and motor symptoms in Parkinson's disease. NPJ Parkinsons Dis 11, 288 (2025).
52. Lin, R., et al. Association of glymphatic system function with peripheral inflammation and motor symptoms in Parkinson's disease. NPJ Parkinsons Dis 11, 62 (2025).
53. Sun, Y.R., Lv, Q.K., Liu, J.Y., Wang, F. & Liu, C.F. New perspectives on the glymphatic system and the relationship between glymphatic system and neurodegenerative diseases. Neurobiol Dis 205, 106791 (2025).
54. Lian, X., et al. Targeting the glymphatic system to promote α-synuclein clearance: a novel therapeutic strategy for Parkinson's disease. Neural Regen Res 21, 233–247 (2026).
55. Jiang, J., Liu, G., Shi, S., Li, Y. & Li, Z. Effects of manual acupuncture combined with donepezil in a mouse model of Alzheimer's disease. Acupunct Med 37, 64–71 (2019).
56. Si, X., et al. Matrix metalloproteinase-9 inhibition prevents aquaporin-4 depolarization-mediated glymphatic dysfunction in Parkinson's disease. J Adv Res 56, 125–136 (2024).

57. Tian, D.Z., Li, N.Q. & Zhai, J. Exploration on even reinforcing-reducing technique of acupuncture. Zhongguo Zhen Jiu 39, 497–500 (2019).
58. Lio, G., Thobois, S., Ballanger, B., Lau, B. & Boulinguez, P. Removing deep brain stimulation artifacts from the electroencephalogram: Issues, recommendations and an open-source toolbox. Clin Neurophysiol 129, 2170–2185 (2018).

Figures

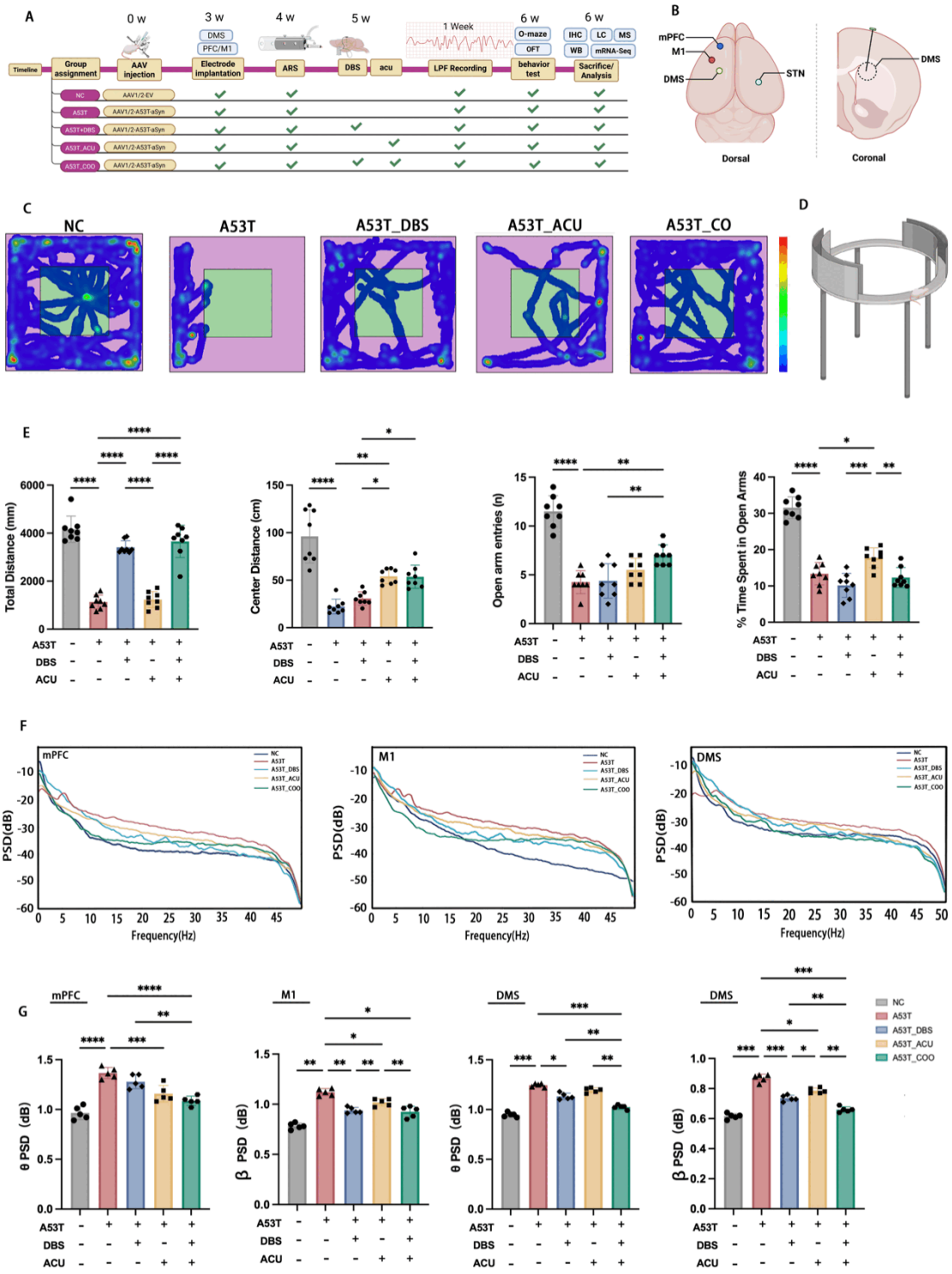


Figure 1

Combined STN-DBS and acupuncture improve behavioural deficits and differentially modulate regional oscillatory power in A53T rats.

(A) Experimental timeline and group allocation for viral injection, electrode implantation, apomorphine rotation screening (ARS), intervention, local field potential (LFP) recording, behavioural testing and

terminal tissue collection. **(B)** Schematic showing recording sites in the medial prefrontal cortex (mPFC), primary motor cortex (M1) and dorsomedial striatum (DMS), and the stimulation site in the subthalamic nucleus (STN). **(C)** Representative open-field movement heatmaps from NC, A53T, A53T_DBS, A53T_ACU and A53T_CO rats. **(D)** Schematic of the elevated zero maze. **(E)** Quantification of open-field and elevated zero-maze performance, including total distance, centre distance, open-arm entries and percentage of time spent in open arms. **(F)** Representative power spectral density (PSD) curves recorded from the mPFC, M1 and DMS across groups. **(G)** Quantification of selected abnormal frequency-band activity, including mPFC θ power, M1 β power, DMS θ power and DMS β power. Data are presented as mean ± SEM; n = 8 rats per group for behavioural analyses and n = 5 rats per group for PSD analyses. Statistical comparisons were performed using one-way ANOVA followed by Tukey's post hoc test. * $P < 0.05$, ** $P < 0.01$, *** $P < 0.001$, **** $P < 0.0001$. NC, normal control; DBS, deep brain stimulation; ACU, acupuncture; CO, combined intervention.

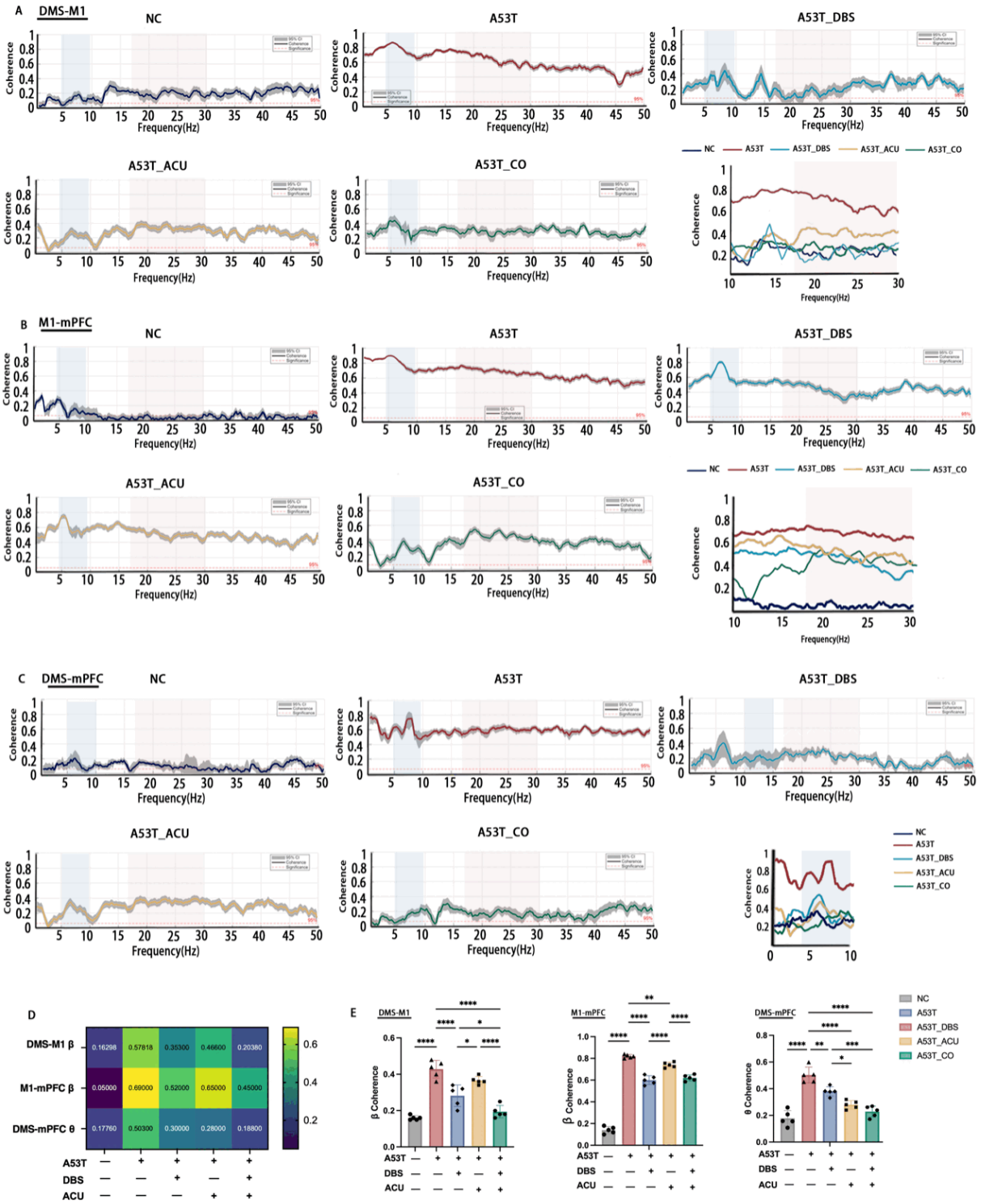


Figure 2

Combined STN-DBS and acupuncture rebalance pathway- and frequency-specific cortico-striatal coherence abnormalities.

(A) Coherence spectra for the DMS–M1 pathway across NC, A53T, A53T_DBS, A53T_ACU and A53T_CO rats, with enlarged traces showing the β-band range. **(B)** Coherence spectra for the M1–mPFC pathway

across groups, with enlarged β-band traces. **(C)** Coherence spectra for the DMS–mPFC pathway across groups, with enlarged θ-band traces. Grey shading indicates the 95% confidence interval, and the dashed red line indicates the significance threshold. **(D)** Heatmap summarizing coherence values in the key abnormal frequency bands, including DMS–M1 β coherence, M1–mPFC β coherence and DMS–mPFC θ coherence. **(E)** Quantification of pathway- and frequency-specific coherence values across groups. Data are presented as mean ± SEM; n = 5 rats per group. Statistical comparisons were performed using one-way ANOVA followed by Tukey's post hoc test. *P < 0.05, **P < 0.01, ***P < 0.001 and ****P < 0.0001. DMS, dorsomedial striatum; M1, primary motor cortex; mPFC, medial prefrontal cortex; DBS, deep brain stimulation; ACU, acupuncture; CO, combined intervention.

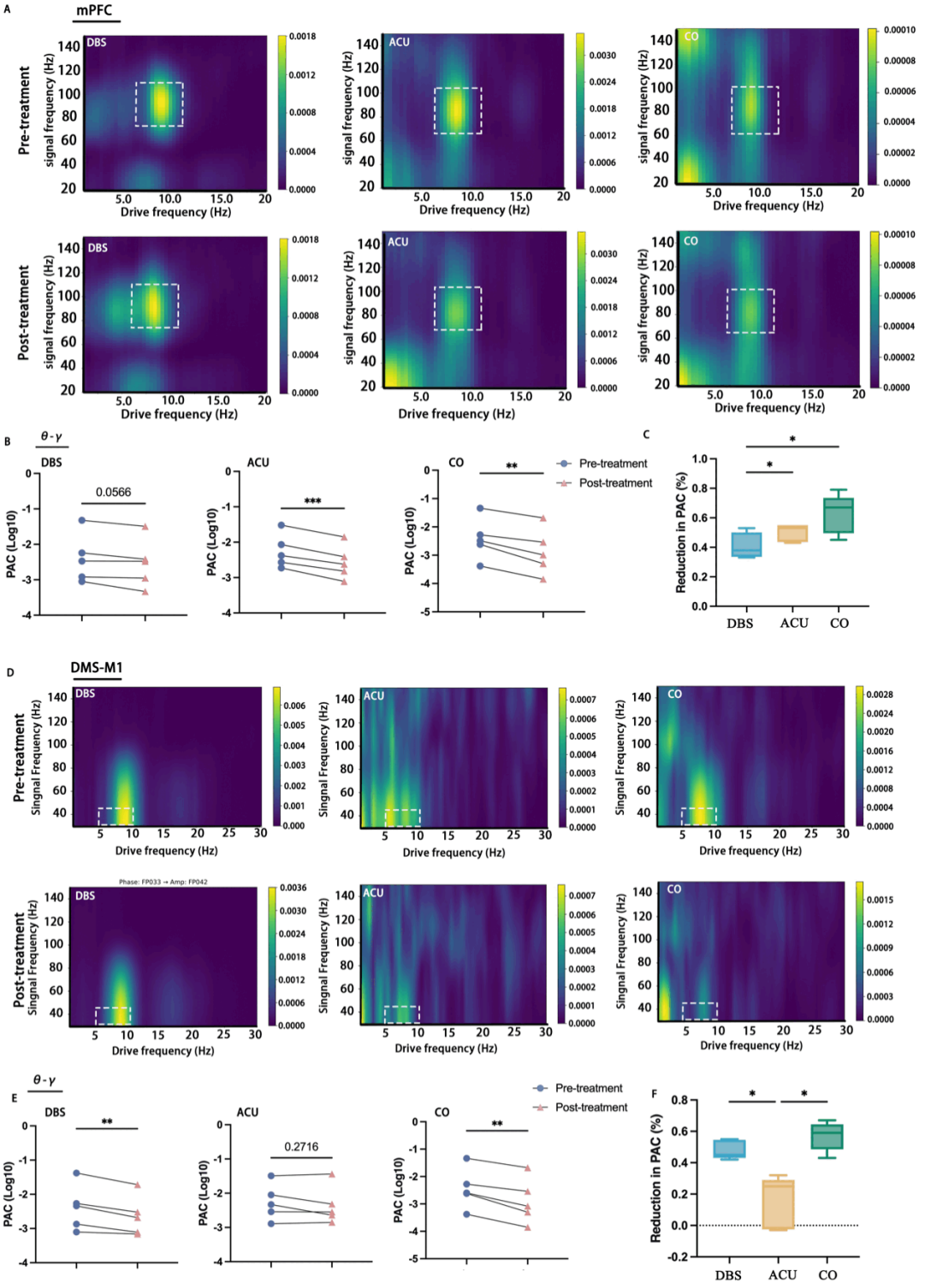
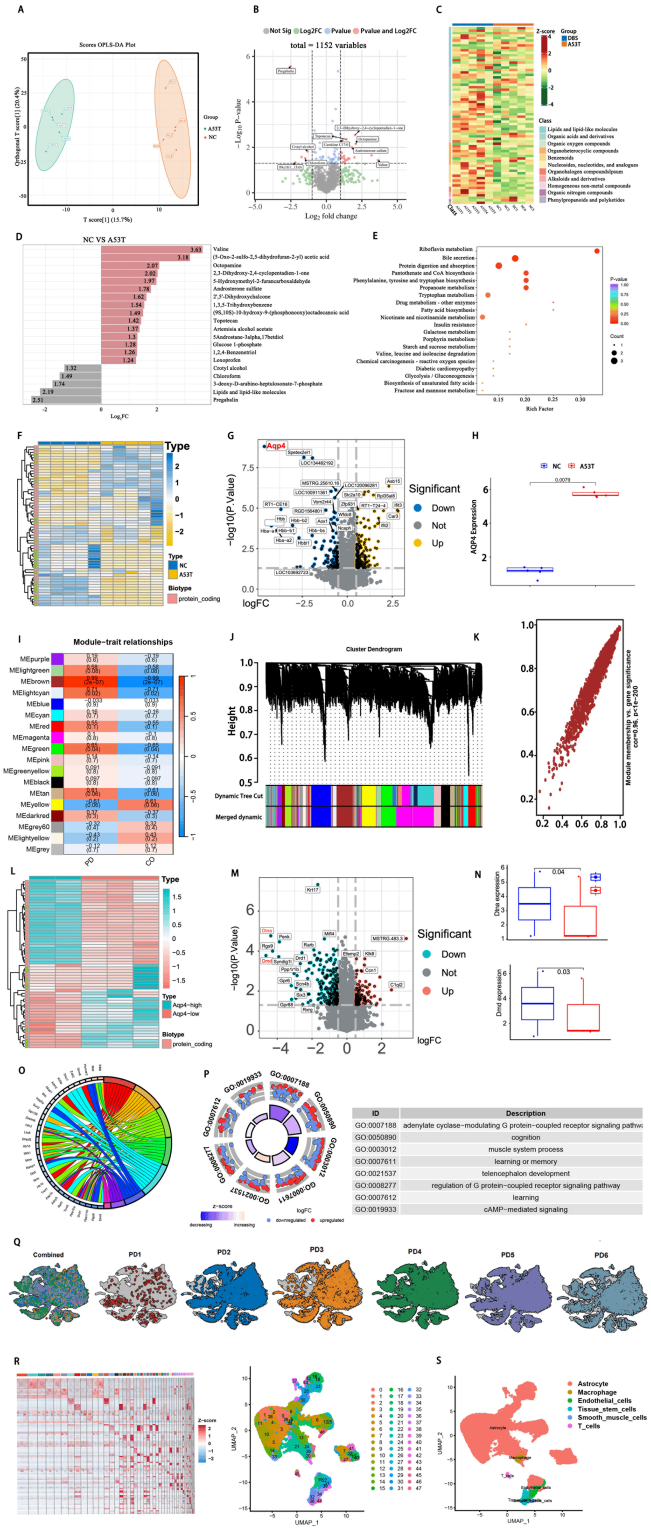


Figure 3

STN-DBS and acupuncture differentially reduce local prefrontal and inter-regional phase–amplitude coupling.

(A) Representative phase–amplitude coupling (PAC) comodulograms in the mPFC before and after treatment in the DBS, ACU and CO groups, showing coupling between θ phase and γ amplitude. Dashed

boxes indicate the θ–γ frequency window used for quantification. **(B)** Paired quantification of mPFC θ–γ PAC before and after treatment in each intervention group. **(C)** Comparison of the relative reduction in mPFC θ–γ PAC among DBS, ACU and CO groups. **(D)** Representative inter-regional PAC comodulograms between the DMS and M1 before and after treatment, showing coupling between DMS θ phase and M1 γ amplitude. Dashed boxes indicate the θ–γ frequency window used for quantification. **(E)** Paired quantification of DMS–M1 θ–γ PAC before and after treatment in each intervention group. **(F)** Comparison of the relative reduction in DMS–M1 θ–γ PAC among DBS, ACU and CO groups. Data are presented as paired individual values in (B) and (E) and as box-and-whisker plots in (C) and (F); n = 5 rats per group. Paired pre- versus post-treatment comparisons were analysed using paired two-tailed t-tests or Wilcoxon matched-pairs tests according to data distribution. Between-group comparisons of PAC reduction were analysed using one-way ANOVA followed by Tukey's post hoc test or Kruskal–Wallis test followed by Dunn's correction, as appropriate. *P < 0.05, **P< 0.01, ***P < 0.001. mPFC, medial prefrontal cortex; DMS, dorsomedial striatum; M1, primary motor cortex; DBS, deep brain stimulation; ACU, acupuncture; CO, combined intervention.



ID	Description
GO:0007188	adenylate cyclase−modulating G protein−coupled receptor signaling pathway
GO:0050890	cognition
GO:0003012	muscle system process
GO:0007611	learning or memory
GO:0021537	telencephalon development
GO:0008277	regulation of G protein−coupled receptor signaling pathway
GO:0007612	learning
GO:0019933	cAMP−mediated signaling

Figure 4

Striatal multi-omic profiling identifies AQP4-associated molecular alterations in A53T rats.

(A) OPLS-DA score plot showing metabolomic separation between NC and A53T rats. **(B)** Volcano plot of differential metabolites between NC and A53T groups. **(C)** Heatmap showing the distribution of differential metabolites by chemical class. **(D)** Bar plot of representative altered metabolites ranked by

log2 fold change. **(E)** Pathway enrichment analysis of differential metabolites. **(F)** Heatmap of differentially expressed genes in striatal transcriptomic data. **(G)** Volcano plot of differentially expressed genes, with Aqp4 highlighted. **(H)** Quantification of Aqp4 expression in NC and A53T rats. **(I)** WGCNA module–trait correlation heatmap. **(J)** Gene clustering dendrogram and merged co-expression modules. **(K)** Correlation between module membership and gene significance in the disease-associated module. **(L)** Heatmap of differentially expressed genes after stratification by Aqp4 expression. **(M)** Volcano plot comparing Aqp4-high and Aqp4-low samples, with glymphatic-associated genes highlighted. **(N)** Expression of Dmd and Dtna in Aqp4-high and Aqp4-low samples. **(O)** Chord plot showing enriched biological processes associated with AQP4-related genes. **(P)** Circular Gene Ontology enrichment plot and corresponding functional terms. **(Q)** UMAP visualization of the public single-cell dataset GSE184950, shown as combined data and individual PD samples. **(R)** Heatmap of marker-gene expression and unsupervised clustering of single-cell populations. **(S)** Cell-type annotation of single-cell clusters. In volcano plots, coloured points indicate significantly upregulated or downregulated features, and grey points indicate non-significant features. Box plots show median and interquartile range. Statistical analyses were performed using differential expression or enrichment methods described in the Methods; P values are shown where applicable. NC, normal control; OPLS-DA, orthogonal partial least-squares discriminant analysis; WGCNA, weighted gene co-expression network analysis; UMAP, uniform manifold approximation and projection; GO, Gene Ontology.

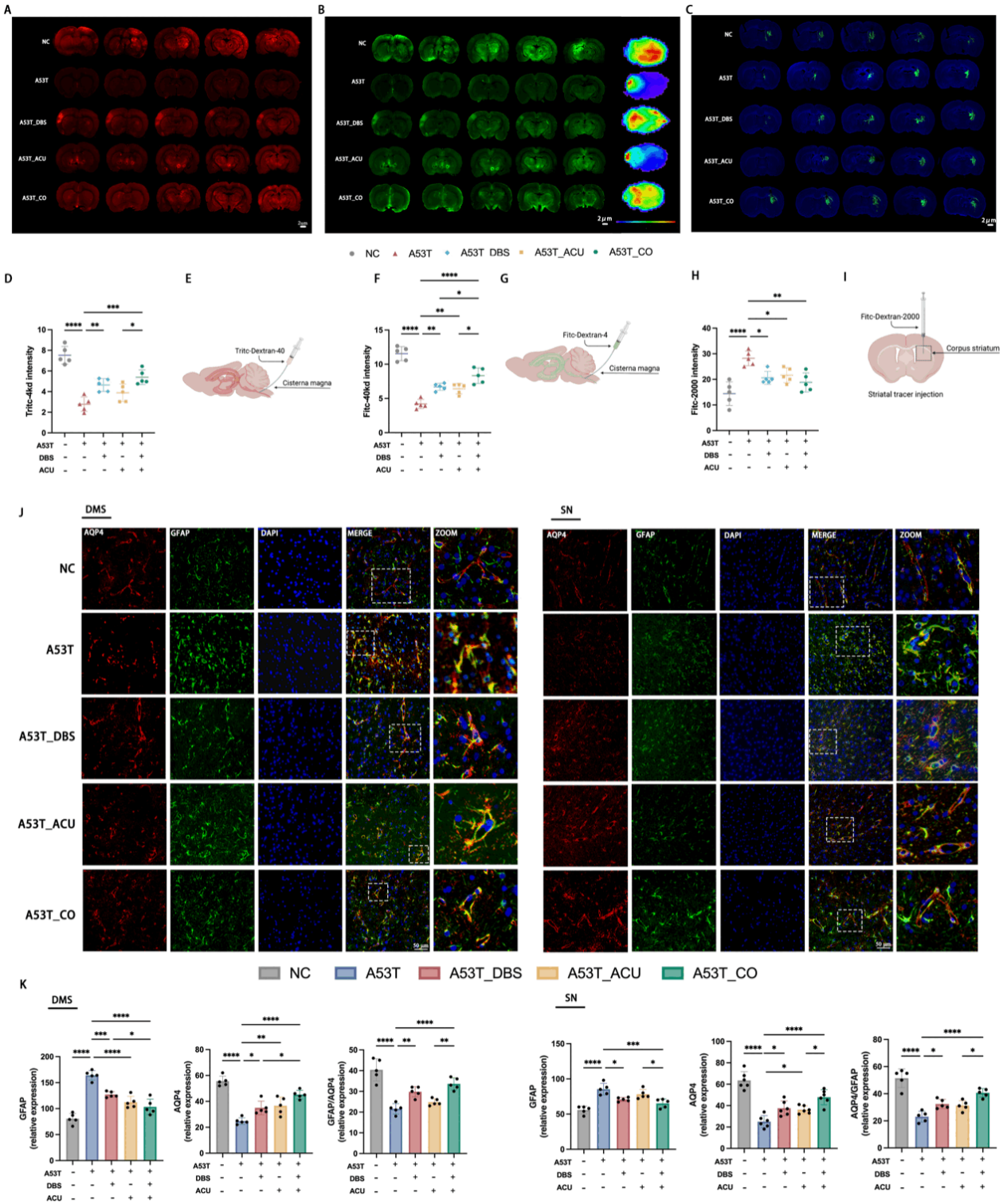


Figure 5

Combined STN-DBS and acupuncture improve glymphatic transport and perivascular AQP4 polarization in A53T rats.

(A) Representative brain sections showing cerebrospinal fluid (CSF) influx of TRITC-labelled 4 kDa dextran after cisterna magna injection across groups. **(B)** Representative brain sections showing CSF

influx of FITC-labelled 40 kDa dextran and corresponding pseudocolour intensity maps. **(C)** Representative brain sections showing striatal retention of FITC-labelled 2000 kDa dextran after intrastriatal injection. **(D)** Quantification of TRITC-labelled 4 kDa dextran influx. **(E)** Schematic of cisterna magna injection for CSF influx assessment. **(F)** Quantification of FITC-labelled 40 kDa dextran influx. **(G)** Schematic of FITC-labelled dextran infusion into the cisterna magna. **(H)** Quantification of FITC-labelled 2000 kDa dextran retention in the striatum. **(I)** Schematic of intrastriatal tracer injection. **(J)** Representative immunofluorescence images of AQP4, GFAP and DAPI staining in the dorsomedial striatum (DMS) and substantia nigra (SN). Boxed regions indicate enlarged areas shown in the zoom panels. Scale bars, 50 μm. **(K)** Quantification of GFAP expression, AQP4 expression and AQP4/GFAP ratio in the DMS and SN. Data are presented as mean ± SEM; n = 5 rats per group. Statistical comparisons were performed using one-way ANOVA followed by Tukey's post hoc test. **P* < 0.05, ***P* < 0.01, *** *P* < 0.001, *****P* < 0.0001. AQP4, aquaporin-4; GFAP, glial fibrillary acidic protein; DAPI, 4',6-diamidino-2-phenylindole; DBS, deep brain stimulation; ACU, acupuncture; CO, combined intervention.

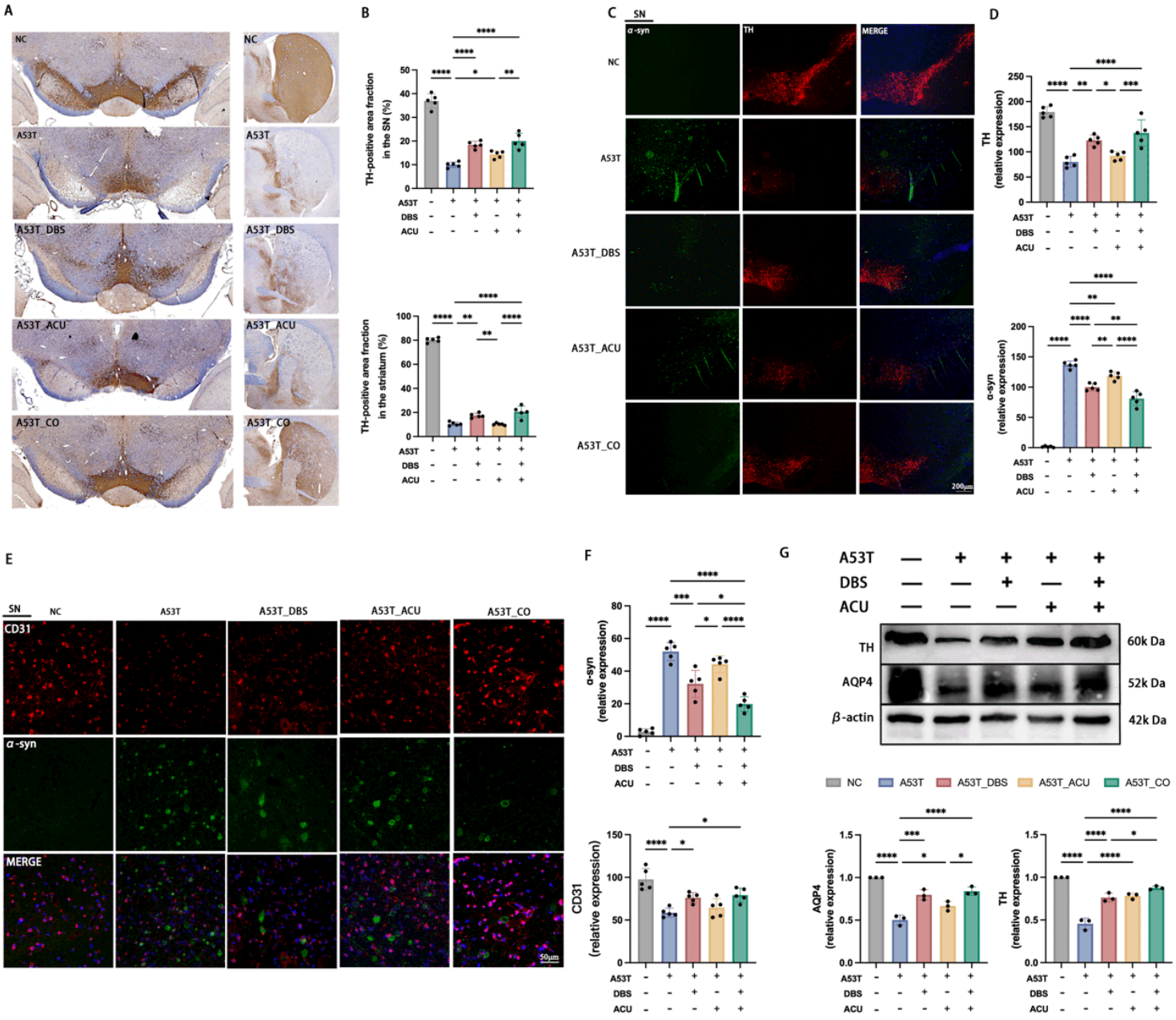


Figure 6

Combined STN-DBS and acupuncture attenuate α-syn pathology and support nigrostriatal preservation.

(A) Representative TH immunohistochemistry images in the substantia nigra (SN) and striatum across NC, A53T, A53T_DBS, A53T_ACU and A53T_CO rats. **(B)** Quantification of TH-positive area fraction in the SN and striatum. **(C)** Representative immunofluorescence images of α-syn and TH in the SN. Scale bar, 200 μm. **(D)** Quantification of TH and α-syn fluorescence intensity in the SN. **(E)** Representative immunofluorescence images of CD31 and α-syn in the SN. Scale bar, 50 μm. **(F)** Quantification of α-syn and CD31 fluorescence intensity in the SN. **(G)** Representative western blots and quantification of striatal TH and AQP4 expression normalized to β-actin. Data are presented as mean ± SEM; n = 5 rats per group for histological and immunofluorescence analyses, and n = 3 rats per group for western blotting.

Statistical comparisons were performed using one-way ANOVA followed by Tukey's post hoc test. *P < 0.05, **P < 0.01, ***P < 0.001, ****P < 0.0001. TH, tyrosine hydroxylase; α-syn, α-synuclein; CD31, platelet endothelial cell adhesion molecule-1; AQP4, aquaporin-4; DBS, deep brain stimulation; ACU, acupuncture; CO, combined intervention.

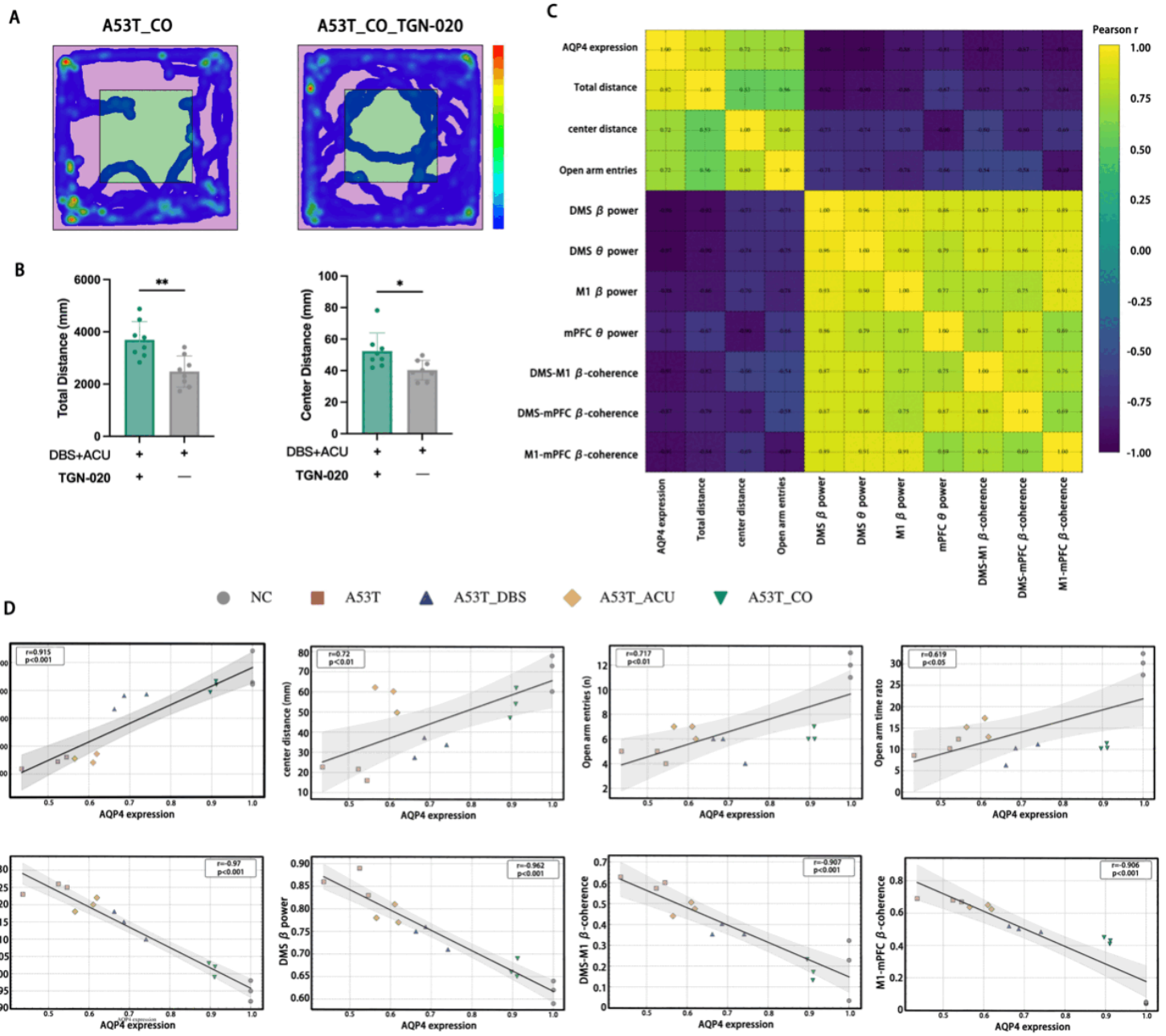


Figure 7

AQP4 inhibition partially attenuates behavioural benefit and links AQP4 expression to behavioural and electrophysiological readouts.

(A) Representative open-field movement heatmaps from A53T_CO rats treated with vehicle or the AQP4 inhibitor TGN-020. **(B)** Quantification of total distance and centre distance in A53T_CO rats with or

without TGN-020 treatment. **(C)** Pearson correlation matrix showing associations among AQP4 expression, behavioural measures, regional oscillatory power and inter-regional coherence. Colour indicates Pearson's correlation coefficient. **(D)** Scatter plots showing representative correlations between AQP4 expression and behavioural or electrophysiological measures, including total distance, centre distance, open-arm entries, open-arm time ratio, DMS θ power, DMS β power, DMS–M1 β coherence and M1–mPFC β coherence. Shaded areas indicate 95% confidence intervals for the fitted regression lines. Data in (B) are presented as mean ± SEM; n = 8 rats per group. Comparisons in (B) were analysed using unpaired two-tailed Student's t-tests or Mann–Whitney U tests according to data distribution. Correlations were analysed using Pearson correlation. *P< 0.05 , **P < 0.01. AQP4, aquaporin 4; DMS, dorsomedial striatum; M1, primary motor cortex; mPFC, medial prefrontal cortex; DBS, deep brain stimulation; ACU, acupuncture; CO, combined intervention.

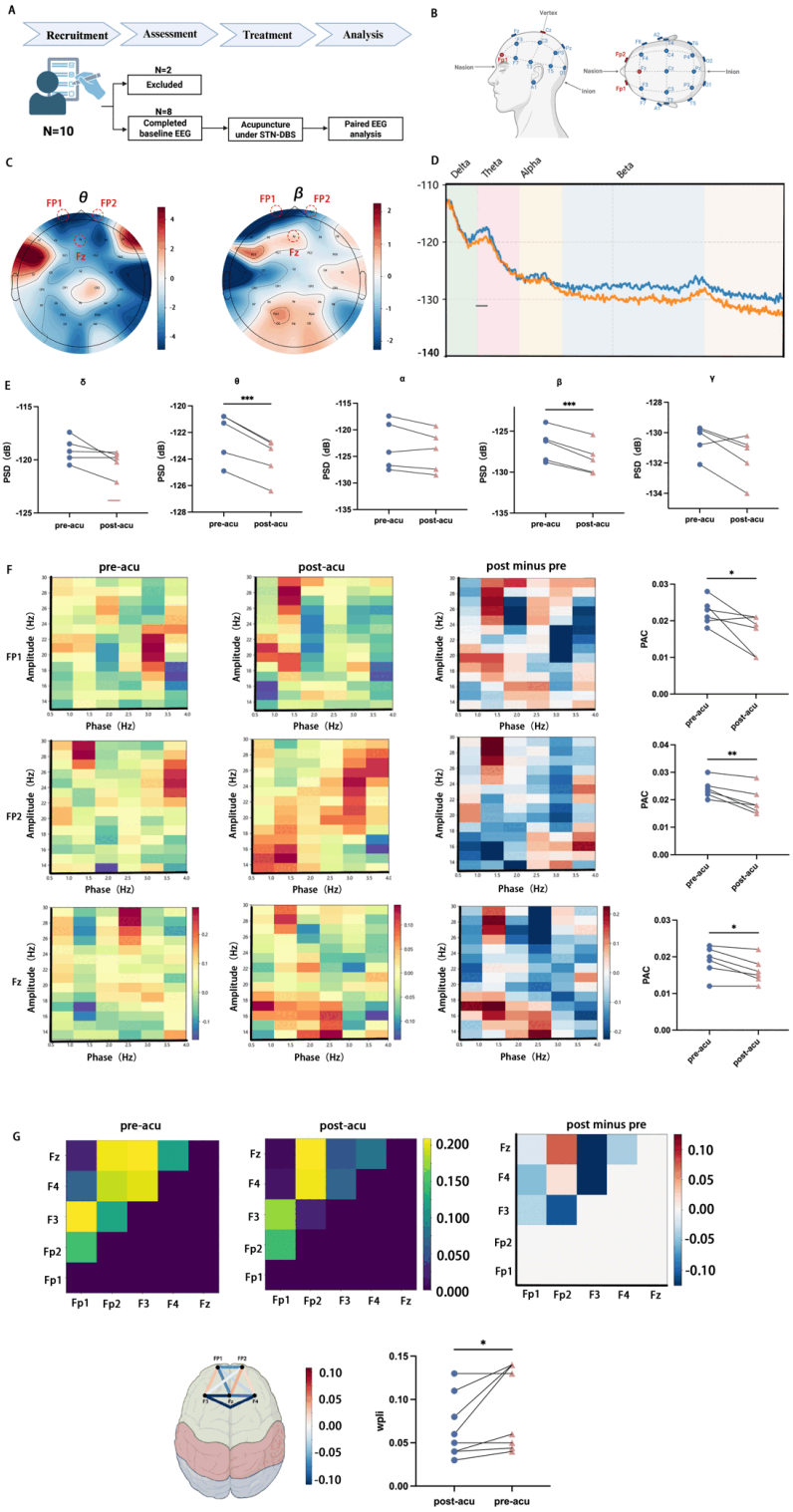


Figure 8

Acupuncture during active STN-DBS modulates prefrontal EEG activity in patients with PD and anxiety.

(A) Workflow of the exploratory clinical EEG study, including recruitment, assessment, acupuncture under active STN-DBS and paired EEG analysis. **(B)** Schematic of the 32-channel EEG montage, highlighting frontal/prefrontal electrodes used for spectral, phase–amplitude coupling (PAC) and

connectivity analyses. **(C)** Topographic maps showing acupuncture-related changes in θ- and β-band power, with frontal/prefrontal electrodes highlighted. **(D)** Representative power spectral density (PSD) curves before and after acupuncture during active STN-DBS. Shaded regions indicate canonical frequency bands. **(E)** Paired quantification of PSD in δ, θ, α, β and γ bands before and after acupuncture. **(F)** PAC maps at Fp1, Fp2 and Fz before and after acupuncture, corresponding post-minus-pre difference maps, and paired quantification of PAC changes. **(G)** Frontal/prefrontal weighted phase-lag index (wPLI) matrices before and after acupuncture, post-minus-pre difference map, schematic representation of altered frontal/prefrontal connectivity and paired quantification of wPLI. Data are presented as paired individual values. Paired comparisons were analysed using paired two-tailed t-tests or Wilcoxon matched-pairs tests according to data distribution. *P< 0.05, **P < 0.01, ***P < 0.001. PD, Parkinson's disease; STN-DBS, subthalamic nucleus deep brain stimulation; EEG, electroencephalography; PSD, power spectral density; PAC, phase–amplitude coupling; wPLI, weighted phase-lag index.

Supplementary Files

This is a list of supplementary files associated with this preprint. Click to download.

- WB.pdf